Int J Adv Manuf Technol (2014) 71:699–710
DOI 10.1007/s00170-013-5521-9

ORIGINAL ARTICLE

Effects of different restraints on the weld-induced residual deformations and stresses in a steel plate

M. Adak · C. Guedes Soares

Received: 13 May 2011 / Accepted: 20 November 2013 / Published online: 7 December 2013

Abstract Effects of three different plate boundary constraints on the residual stress field and deformation are investigated numerically during butt-joint welding. For the numerical solution of the heat transfer equations, the finite element method is used to predict the temperature profile as well as residual stress field due to three different plate boundary conditions. The distortion of the welded plate is modeled as a nonlinear problem in geometry and material, adopting a finite element solution based upon the thermo–elastic–plastic large deflection theory. High-strength shipbuilding steel AH36 with temperature-depending material properties and nonlinear stress–strain material properties (bilinear isotropic hardening option uses the von Mises yield criteria) are assumed for the numerical analysis. For verifying the results, the temperature profile is compared with the result obtained in a previous research. In the mechanical analysis, three different boundary conditions are applied. Effects of plate thickness, plate width, and mesh model on the residual stress with boundary constraint are studied.

Keywords Welding residual stress · Temperature distribution · Finite element analysis · Bilinear isotropic hardening

Nomenclature

T	Temperature (°C)
T_0	Room temperature (°C)
T_1	Constant temperature at weld pool (°C)
ρ	Density of the base metal (kilogram per cubic meter)
C	Specific heat (joules per kilogram kelvin)
k	Thermal conductivity (W/m K)
$\underline{t}$	Time
h	Convective heat transfer coefficient (watts per square meter kelvin)
x, y, z	Coordinates
σ	Stress vector
ε	Total strain vector
ε^{e}	Elastic strain vector
ε^{p}	Plastic strain vector
ε^{t}	Thermal strain vector

M. Adak · C. Guedes Soares (✉)
Centre for Marine Technology and Engineering (CENTEC), University of Lisbon, Instituto Superior Técnico, Lisbon, Portugal
e-mail: guedess@mar.ist.utl.pt

1 Introduction

When a material is heated with initial high temperature in a weld joint, the highly localized transient heat and strongly nonlinear temperature fields in both heating and cooling processes cause nonuniform thermal expansion and contraction and thus result in plastic deformation in the weld and surrounding areas. During welding, one edge of the plate can be assumed to be fixed to reduce the deformation and this induces stress due to fixed constraints.

Due to the complexity of the physical processes involved in welding, however, simple mathematical solutions can not address the practical manufacturing process. Furthermore, it is also impossible for any experimental technique to obtain a complete mapping of the residual stress and distortion distribution in a general welded structure.

The research activity in welding simulation started decades ago. Rosenthal [18] was among the first researchers to develop an analytical solution of heat flow during welding based on conduction heat transfer for predicting the shape of the weld pool for two- and three-dimensional welds. Watanabe and Satoh [24] used the analytical solutions resulting from the theory of elasticity for the prediction of thermal deformations

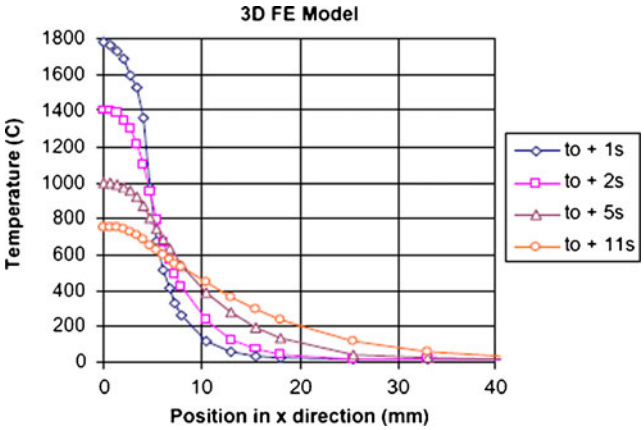

Fig. 1 Temperature along transverse direction (x-axis) from ref. [13]

due to welding and line heating. However, since elastic solutions are limited, application of the method is also limited.

First, the numerical application (2D finite element analysis) was reported by Hibbitt and Marcal [9] to predict residual stresses in a welded plate. Due to computational and cost limitations, FE simulation efforts during the 1970s and 1980s were focused on simplified 2D geometries by Karlsson [11] and Masubuchi [15]. In reality, the thermal and stress–strain responses of all weldments are three-dimensional (3D). With the increasing computational power of present-day computers, numerical methods based on finite element and finite difference schemes have been extensively used. Kristina et al. [12], Argyris and Szimmat [5], Rybicki et al. [19], Papazoglou and Masubuchi [17], and Murakawa et al. [16] worked out thermo–elasto–plastic problems using high-speed workstations but the resulting deformations showed poor accuracy compared to the experimental results. More complex 3D welding simulation was conducted using commercial FEA software which was reported by Tekriwal and Mazumder [21, 22] and Dong et al. [7].

Al-Mulhim et al. [3] and Sunar et al. [20] investigated thermal and stress analysis with constant heat source at weld pool and constant material properties during welding in case of 2D problem. Biswas et al. [6] modeled the angular distortion using a plasticity-based distortion welding. Adak and Mandal [1, 2] used the pseudolinear equivalent constant stiffness system to predict the temperature distribution and deformation shape after welding. It is clear from the literature survey that most of them have concentrated on 2D and 3D simulation process for deformation shape and residual field due to welding without boundary constraints.

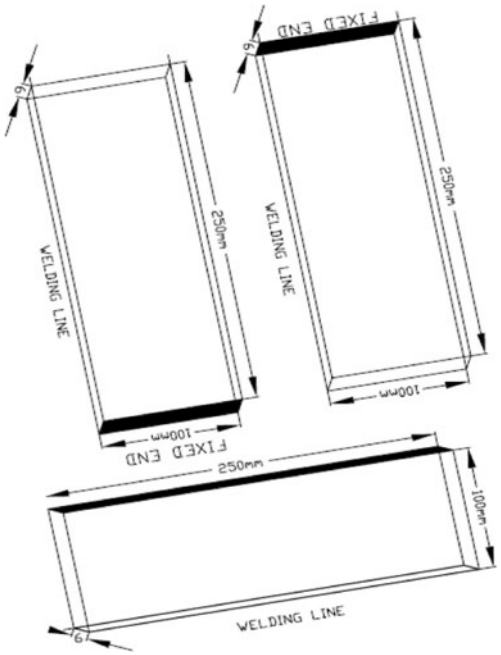

Fig. 3 Variation of location for boundary constraints

Not only the welding residual stress and distortion have been studied by welding researchers, but also the effect of welding parameters, welding sequence, and welding joint geometry. Teng et al. [23] and Ji et al. [10] investigated the distortion mechanism and the effects of welding sequence on thin panel distortions using a finite element analysis approach. Zhu and Chao [25] investigated the effect of each

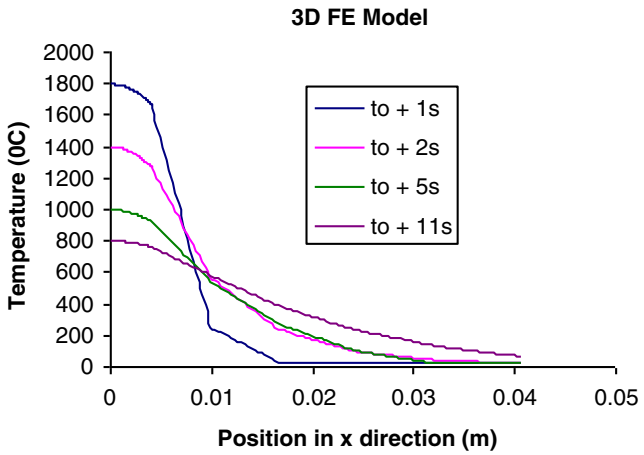

Fig. 2 Temperature along transverse direction (x-axis) calculated here

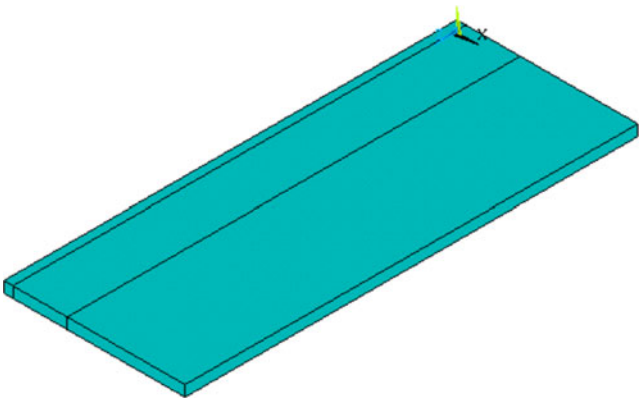

Fig. 4 Specimen for analysis

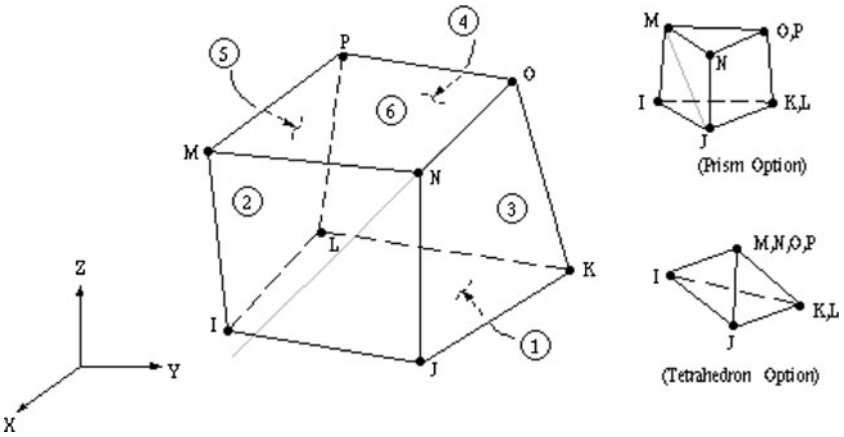

Fig. 5 Element type

temperature-dependent material property on the transient temperature, residual stress by using finite element analyses approach.

Some researchers have already investigated the effects on residual stresses due to different boundary conditions such as Fanous et al. [8], who simulated the effects on residual stresses by choosing the appropriate boundary conditions in modeling the welding process. Three boundary condition sets were considered; in the first boundary condition set, the plates are welded along the joining side with a clamp at one end, after which the plates are released and checked for residual stresses. In the second boundary condition set, the plates are welded with a large structure so that the plate may expand freely but with no rotation allowed throughout the process. In the third set, the structural boundary condition is the same as that of set 1 but with a decrease in the thermal load. It is observed that the stresses generated during the welding process are not highly affected by the change in boundary conditions. Sunar et al. [20] investigated the effect on residual stress due to fixed end along welding direction. In that case, maximum magnitude of von Mises stress is lesser than the yield strength of the substrate material for all the heating durations.

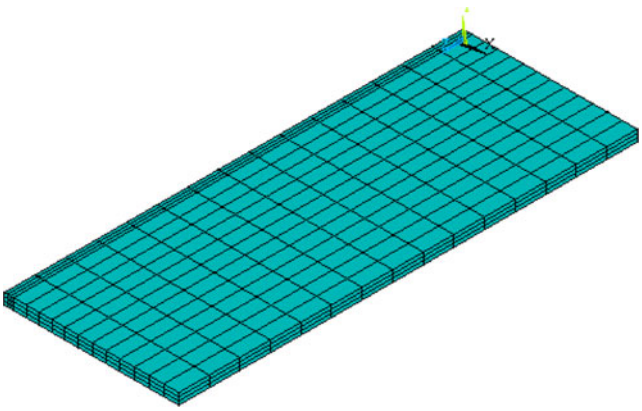

Fig. 6 The mesh in the half of symmetry plate

From the literature survey, it is demonstrated that it is most important to apply the suitable boundary conditions during welding process. In this study, three different types of boundary conditions are applied to reduce the welding distortions and their effects on residual stresses are investigated. Three boundary conditions are considered as case1: the nodes at the extreme end from the weld line are constrained; case 2: the nodes at the edge along x-axis (bottom) are constrained; and case 3: the nodes at the edge parallel to the x-axis (top) are constrained. From the literature survey, it is clear that the finite element method (FEM) has been successfully used to evaluate the thermo–mechanical response of the complex welding process. Therefore, in this paper, the finite element method (ANSYS software package) has been used to simulate the arc welding process.

2 Verification of butt-welding analysis using finite element analysis

In this study, no experimental data are available to verify the simulation results and thus the results of the simulation are compared to numerical results obtained in a previous research. After validating the simulation results with the numerical results, the same finite element modeling is used to simulate the welding process throughout this study.

A finite element simulation of a simple butt-joint welding for 3D model is verified comparing with the work of Long et al. [13]. To do this, a simple butt-joint welding, whose welding parameters are consistent to those of Long's model, was simulated by using the ANSYS finite element code. The model then is verified by comparison of its temperature distribution at some chosen nodes with the Long's model. The temperature-dependent material properties for the thermal and mechanical analyses were equivalent to those used in Long's analyses. Plate geometry of the butt-joint welding is similar to Long's model (Fig. 1).

Table 1 Steel density versus temperature

°C	Kg/m^3
25	7,800
1,450	7,438
3,000	7,438

The results show that the temperature histories at various locations from the weld line are in reasonable agreement with the result obtained by Long et al. [13]. The peak temperatures for both models are almost identical. The distances from the weld line of the verification model are slightly different from Long's possibly due to the mesh size. Figures 2 and 3 show the temperature distribution curves from Long's and verification models, respectively.

In the present study, the same type of model and procedure have been followed which are described in the following sections.

3 Numerical simulation procedure

The finite element simulation of welding process requires two analyses; transient thermal analysis and elasto–plastic analysis. To simplify the simulation procedure, uncoupled numerical simulations are used. In such uncoupled analyses, the results of the transient thermal analysis which include the temperature distribution, which will be used for the second analysis together with the temperature-dependent mechanical properties of the material, i.e., thermal expansion coefficient, modulus of elasticity, Poisson's ratio, density, etc. To simplify the numerical process, simple heat source model as a constant temperature is considered at the welding zone according to Sunar et al. [20].

3.1 Mathematical modeling

The mathematical models for the temperature and stress fields are given under the appropriate sub-headings.

3.1.1 Thermal analysis

The mathematical model can be used three-dimensionally since the plate is considered with thickness. The conduction heating of the solid with constant temperature source at the fixed end is considered to simulate the welding process for 2-D problem reported by Al-Mulhim et al. [3] and Sunar et al. [20]. Here, the 3D transient heat conduction equation for a rectangular plate heated at one side can be written as

$$\rho C\frac{\partial T}{\partial t}=\frac{\partial}{\partial x}\left(k_x\frac{\partial T}{\partial x}\right)+\frac{\partial}{\partial y}\left(k_y\frac{\partial T}{\partial y}\right)+\frac{\partial}{\partial z}\left(k_z\frac{\partial T}{\partial z}\right)$$

where ρ, C, and k are density, specific heat, and thermal conductivity as a function, respectively.

In case of thermal analysis, at time zero, a uniform temperature that means room temperature is assumed as initial condition except in the weld pool region.

At time $t=0$, $T(x, y, z) = T_0$ and $T(x, y, z) = T_1$ (fixed temperature for weld pool) (according to Sunar et. al., [20]).

At the free surface, except in the weld pool of the rectangular plate (Fig. 4), convection boundary conditions are considered. Therefore, on the surface along the x-axis and parallel to the x-axis,

$$k_z\frac{\partial T}{\partial z}=h(T-T_{amb});$$

Along the weld pool, T = constant (specific temperature);
On the surface parallel to z-axis, $k_x\frac{\partial T}{\partial x}=h(T-T_{amb})$;
On the surface top and bottom surface, $k_y\frac{\partial T}{\partial y}=h(T-T_{amb})$;
where h is the convection coefficient.

The heat exchange between the welded plate and its surroundings during welding and, subsequently, cooling takes place by both convection and radiation. In the thermal model, the convection coefficient $h=15$ W m^{-2}, emissivity $\varepsilon=0.9$

Table 2 Steel thermal conductivity versus temperature

°C	W/m °C
25	55
750	29
800	25.4
1,450	31
3,000	31

Table 3 Steel-specific heat versus temperature

°C	J/kg °C
25	388
700	894
740	1,234
860	610
1,450	814
3,000	814

Table 4 Thermal expansion of steel versus temp

°C	(10^{-6}/°C)
25	12
1,450	14
3,000	14

Table 5 Elastic modulus and Poisson's ratio of steel versus temp

°C	GPa	–
25	206	0.296
100	203	0.311
200	201	0.330
300	200	0.349
400	165	0.367
500	100	0.385
600	60	0.405
700	40	0.423
800	30	0.442
900	20	0.461
1,000	10	0.480
3,000	10	0.480

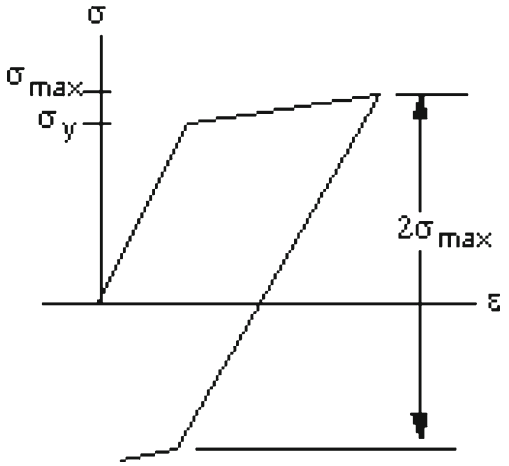

Fig. 8 Bilinear isotropic hardening

and the Stefan–Boltzmann constant=5.669×10^{-8} W $m^{-2}°C^{-4}$ are considered by Long et al. [13]. These thermal boundary conditions are applied for all surfaces of the welding plate except for the symmetrical plane of the plate.

3.1.2 Mechanical analysis

To evaluate the distortion and residual stress distribution, the heat transfer analysis was performed first in order to find nodal temperatures as a function of time. Then, in the second part of the analyses, a nonlinear structural analysis was carried using the temperature distributions, which were obtained from the heat transfer analysis.

During the welding procedure, the heating is localized and, therefore, a very large temperature variation occurs over a small region. Consequently, considerable thermal stresses are generated due to the thermal gradient. In the present study, the stress–strain relationship is defined as follows:

$$\{\sigma\} = [D]\{\varepsilon_e\}$$

where $\{\sigma\}$ is the stress vector, $[D]$ is the stiffness matrix, and $\{\varepsilon_e\}$ is the elastic strain vector.

For the deformation of metals, the von Mises yield criterion is employed and the elastic strain is given by

$$\varepsilon_e = \varepsilon - \varepsilon_{pl} - \varepsilon_{th}$$

where ε_e is the elastic strain, ε is the total strain, ε_{pl} is the plastic strain, and ε_{th} is the thermal strain.

The stress–strain relationship now becomes

$$\{\sigma\} = [D]\left(\{\varepsilon\} - \{\varepsilon_{pl}\} - \{\varepsilon_{th}\}\right)$$

The structural analysis causes the stress due to thermal gradient and the fixed edge. A rate-independent thermo–

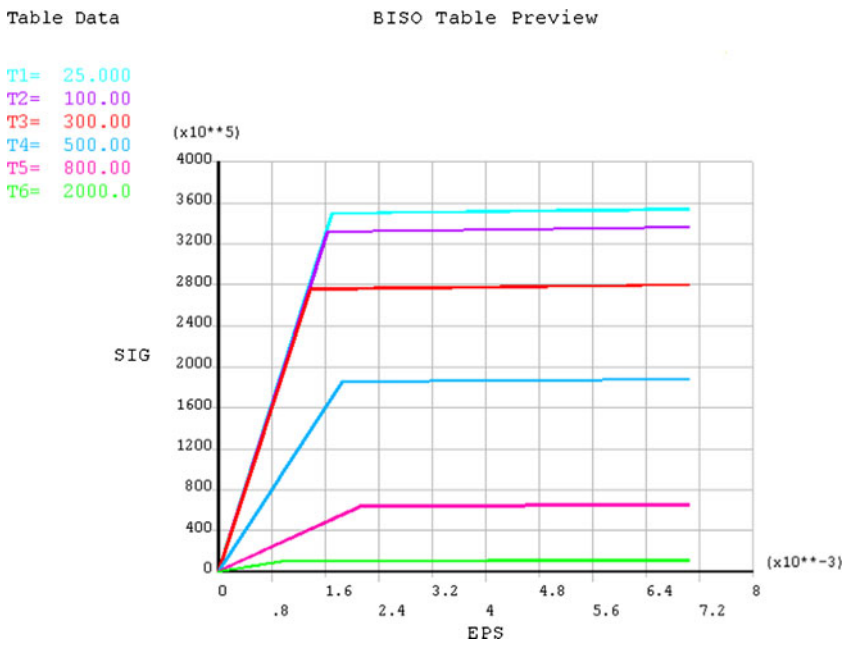

Fig. 7 Stress–strain behavior of steel at different temperatures

elasto–plastic material model with temperature-dependent material properties are incorporated into the finite element modeling.

In the case of mechanical analysis, three cases for boundary constraints are considered.

Case 1 The nodes at the extreme end from the weld line are constrained. Symmetry boundary condition is applied at the weld line as shown in Fig. 3.

Case 2 The nodes at the edge along the x-axis (bottom) are constrained. Symmetry boundary condition is applied at the weld line as shown in Fig. 3.

Case 3 The nodes at the edge parallel to the x-axis (top) are constrained. Symmetry boundary condition is applied at the weld line shown in Fig. 3. These three cases are solved for residual stresses in mechanical response.

3.2 Methodology of the numerical simulation

The ANSYS program [4] is used to conduct the stress analysis of the high-strength rectangular plate with different fixed edges. The following procedures are adopted for the simulations.

The first part of the finite element simulation is heat transfer analysis. In the finite element formulation, the heat conduction equation can be written for each element as follows:

3.2.1 Applying Galerkin criterion

$$\int_v \left[N_i \frac{\partial}{\partial x}\left(k_x \frac{\partial \overline{T}}{\partial x}\right) + N_i \frac{\partial}{\partial y}\left(k_y \frac{\partial \overline{T}}{\partial y}\right) + N_i \frac{\partial}{\partial z}\left(k_z \frac{\partial \overline{T}}{\partial z}\right)\right] dxdydz = \int_v N_i \rho c \frac{\partial \overline{T}}{\partial t} dxdydz$$

Assume $T \sim \overline{T} = \sum_{i=1}^{r} N_i T_i = [N]\{T\}$

3.2.2 Final equation takes form by using boundary conditions

$$[C]\frac{d\{T\}}{dt} = [K]\{T\}$$

where $[C]$ is the specific heat matrix, $[K]$ is the conductivity matrix, $\{T\}$ is the vector of nodal temperature, $d\{T\}/dt$ is vector of time derivative of $\{T\}$.

3.2.3 Convergence and stability scheme

The terms $\frac{dT}{dt}$ and T are written in various forms in different time stepping schemes.

$$[C]\left\{\frac{T(t+\Delta t)-T(t)}{\Delta t}\right\} = [K]\{\theta T(t+\Delta t) + (1-\theta)T(t)\}$$

This analysis requires an integration of the heat conduction equation with respect to time. The Crank–Nicolson theta integration ($\theta = 1/2$) scheme is tested for convergence and stability.

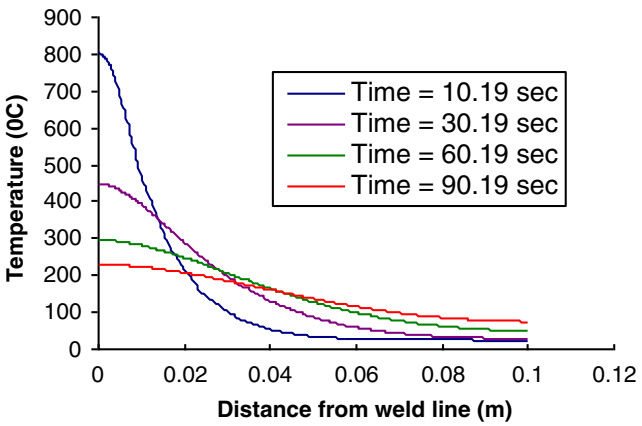

Fig. 9 Temperature distribution along the centerline at various moments in time

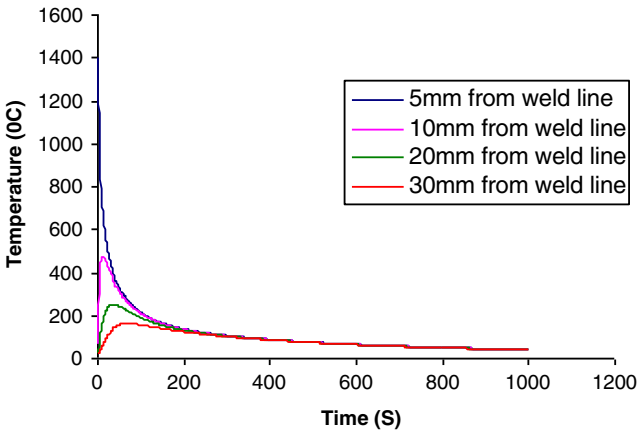

Fig. 10 Transient temperature distribution at various points in transverse direction

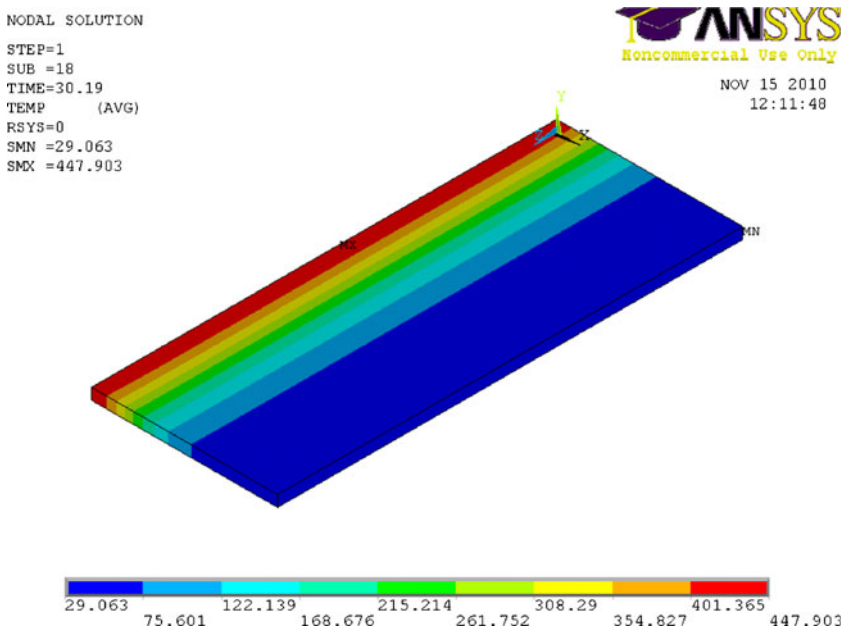

Fig. 11 Temperature contour in °C for 30.19-s heating duration

For the numerical simulation, a rectangular 3D plate, which is symmetric with respect to the welding line is assumed. So, for the analysis to reduce the calculation time, half symmetry of the plate with length 250 mm (z-direction), width 100 mm (x-direction), and thickness 6 mm (y-direction) is considered which is shown in Fig. 4.

Element type For thermal analysis, a 3D 8-node element (SOLID 70) with three degrees of freedom at each node (translations in the nodal x, y, and z directions) is used, and for structural analysis, the element type is SOLID 185. The element has plasticity, creep, swelling, stress stiffening, large deflection, and large strain capacities. This choice was arrived at often a parametric study using different element types shown in Fig. 5, which led to the conclusion that choosing an element having both thermal and structural characteristics is, according to experience, not optimal.

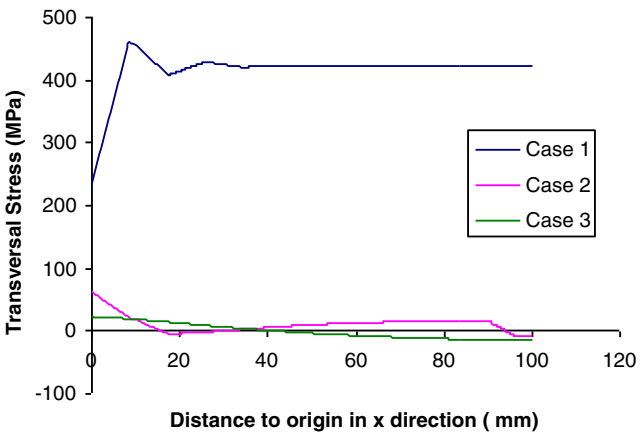

Fig. 12 Transverse stresses along x at middle of plate

Mesh generation In order to generate the system of equations, as well as to find the result at each point of the rectangular plate, a mesh is generated throughout the volume. In order to achieve this, the ANSYS program allows for control of the size and geometry of the mesh in order to obtain the most precise solution. However, a very large number of grid points can compromise the computer's capacity. Figure 6 shows the mesh in the symmetry half of the rectangular plate. Welding direction being z-axis, sharp temperature gradients are expected along both x- and y-axes. Therefore, a very fine grid has been adopted in the weld bead region; finer mesh grid has been chosen away from weld region and course grid is chosen along welding direction (z-axis) (Fig. 6).

Material properties In this numerical simulation, temperature-dependent material properties are used. Steel grade AH36 (high-strength shipbuilding steel) is implemented with temperature dependent on properties as specified in Tables 1, 2, 3, 4, 5 and Fig. 7 Marstruct [14].

The bilinear isotropic hardening option was adopted and it uses the von Mises yield criteria coupled with an isotropic work hardening assumption shown in Fig. 8. This option is often preferred for large strain analyses. The material behavior is described by a bilinear stress–strain curve starting at the origin with positive stress and strain values. The initial slope of the curve is taken as the elastic modulus of the material. At the specified yield stress, the curve continues along the second slope defined by the tangent modulus (having the same units as the elastic modulus). The tangent modulus can not be less than zero nor greater than the elastic modulus.

Birth and death feature The material deposition is modeled using an element "birth and death" technique. To achieve the

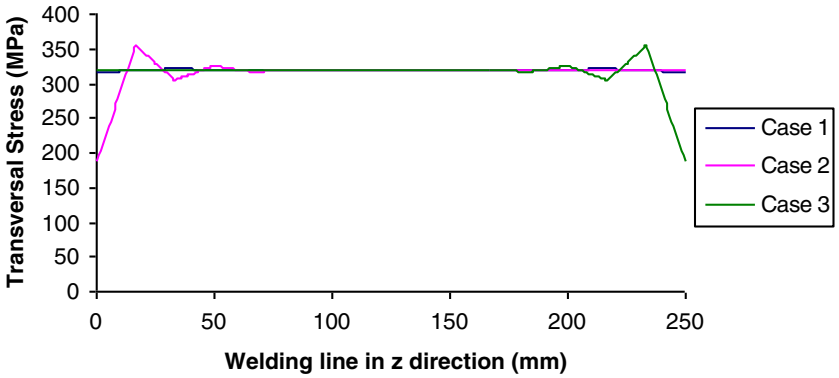

Fig. 13 Transverse stresses along welding line

death element effect, ANSYS code does not actually remove the element from the model. Instead, the weld elements are first deactivated by multiplying their stiffness by a huge reduction factor. Meanwhile, to obtain the birth element effect, the ANSY S program reactivates the death element by allowing its stiffness, element load, etc. return to their original values.

4 Results and discussions

4.1 Temperature time history

In thermal analysis, constant temperature is assumed for simplifying the heat source model at the butt-joint of plate during the welding process. In the thermal model, the heat exchange between the welded plate and its surroundings during welding and, subsequently, cooling takes place by both convection and radiation. The model is used for thermo–mechanical analysis with dimensions 250×100×6 mm for 6-mm thick plate. Temperature fields are obtained numerically and the corresponding stress fields with boundary constraint for three different cases are obtained using the finite element analysis. Temperature-dependent material properties for thermo–mechanical analysis are mentioned in the above tables.

The temperature distributions in the transverse direction (perpendicular to welding line) at the center of the welded plate for different heating periods are shown in Fig. 9. This figure shows that peak temperature is high at the welding line and the temperature is gradually decreasing along the x-axis due to cooling phase. At different time steps, the same pattern is appearing in the temperature history and it is changed in the same place at different moments. Figure 10 shows that during welding and heating treatment, transient temperature distribution is changed at the same time in different places. The temperature profile along the transverse direction, repeats itself till the entire plate cools down to room temperature.

The contour plot in Fig. 11 shows that the temperature at the weld zone is very high and it is gradually decreased away from the weld zone for a particular moment throughout the plate. These changes of transient temperature will significantly affect the forming and developing of the residual stresses.

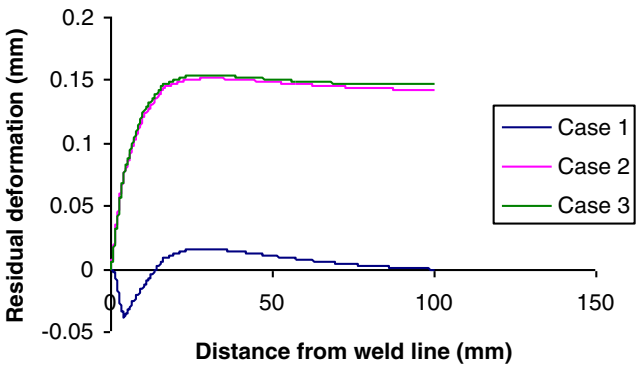

Fig. 14 Deflection along the x-axis at middle of the plate

4.2 Welding residual stress and deformation for three cases

In the mechanical analysis, the large deformation theory is used to simulate the welding residual stress in the butt-welded joint plate. Three boundary constraints are applied for different cases in mechanical analysis and their effects are observed. The results for different boundary conditions show a significant influence on transversal stresses, especially regarding a path transverse to welding direction at a center of plate shown in Fig. 12. From the transverse stress calculation of the three cases, it is clear that the stress level is very low about 70 MPa for both transverse boundary influences in cases 2 and 3, but the stress level for the boundary condition, which is parallel to the welding line in case 1 is high, about 460 MPa.

Those differences result from the fact that the plate having no constraints at $x=100$ mm can deform freely in this direction therefore it will have smaller stress. Transverse stresses are decreased with free ends. It is assumed that with increasing length, this positive effect on local stress development will be negligible. For this simulation, the length of the plate is 100 mm, which means the influence of boundary changing at the plate end is large and may be reasonable for decreased local transverse stresses.

Along the welding line, transversal stresses show almost no differences and are below yield strength. Transverse stresses

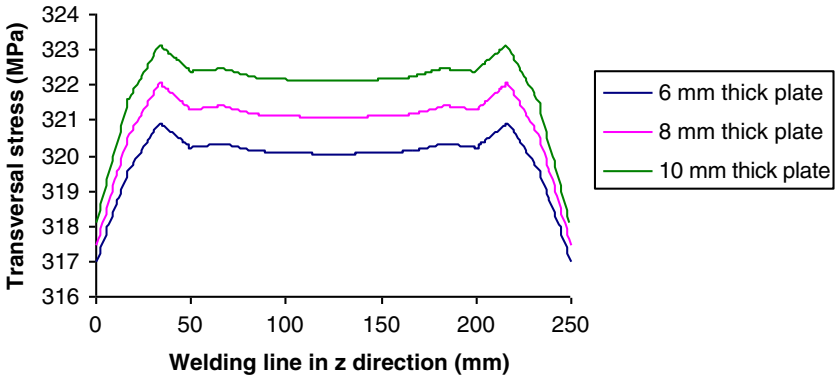

Fig. 15 Transverse stresses along welding line in case 1 with different plate thickness

(Fig. 13), however, present different stress levels at the beginning as well as at the end of the weld.

Figure 14 shows the residual deformation along x-axis at middle of the plate for three different cases. In case 1, the deformation is very much smaller than in the other two cases. In cases 2 and 3, the deformations are almost the same, despite a high value of deformation around 0.15 mm which may be negligible. Therefore, the three different boundary constraints help in reducing the residual deformations; but for case 1, the residual stress is as high as the yield strength of the plate.

From Fig. 13, it is clear that transversal stresses along the welding line are almost identical in the three cases. Therefore, effects of welding parameters (plate thickness, material properties, different mesh model) on residual stresses are investigated due to case 1.

Figure 15 shows the transversal stresses along the welding line in the 6-, 8-, and 10-mm thick plates with constant heat input. From the figure, one can say that transverse stresses are increasing with increasing the plate thickness in case 1.

The effect of mesh refinement in the weld area is studied. The new model with refined meshes consists of 7,425 nodes while the present model consists of 3,520 nodes. Results of the distributions of the transversal residual stress along welding direction for the two mesh densities with the same material model and geometry are displayed in Fig. 16. Very little difference in the results between these two different mesh models is found.

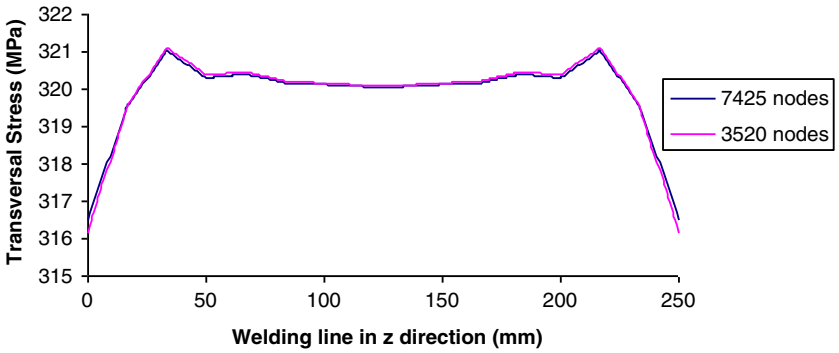

Fig. 16 Transverse stresses along welding line in case 1 with different mesh size

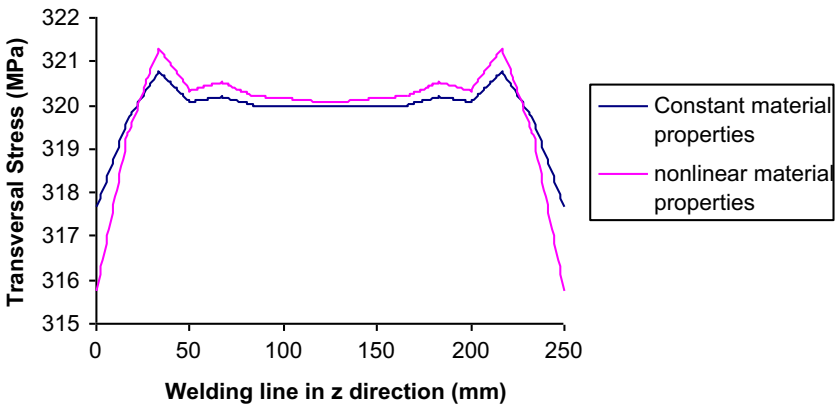

Fig. 17 Transverse stresses along welding line in case 1 with different material properties

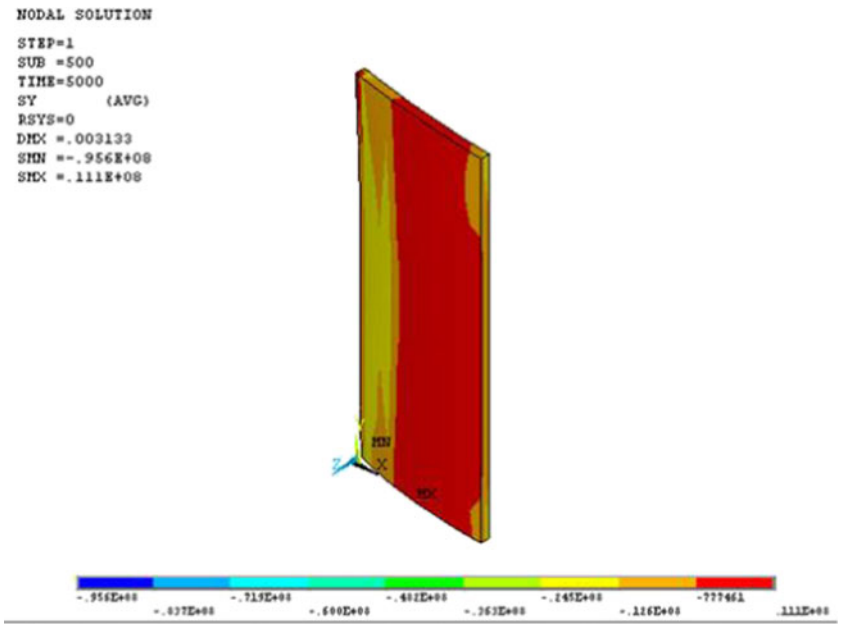

Fig. 18 Residual stress plot along *y*-axis (case1)

Constant material properties according to Sunar et al. [20] and nonlinear material properties (Tables 1, 2, 3, 4, and 5) are considered to investigate the residual stress for 6-mm plate with boundary condition in case 1. Figure 17 shows the effect of different material properties on residual stresses indicating that transversal stresses are higher in case of nonlinear material properties along the welding line, but the stress values are less than the yield stress.

High tensile residual stress field make a crack on a steel plate. Residual stress plots along the *y*-axis are shown in Figs. 18, 19, and 20 for case 1 (end edge of plate parallel to welding line is fixed), case 2 (bottom edge of plate is fixed), and case 3 (top edge of plate is fixed), respectively. These residual stress plots show that the maximum stress values are less than the ultimate tensile stress limit.

5 Conclusions

Thermo–elastic–plastic FEM is used to simulate the welding temperature field and the influences of three different boundary constraints along different edges on the residual stress field in a high-strength butt-joint steel plate.

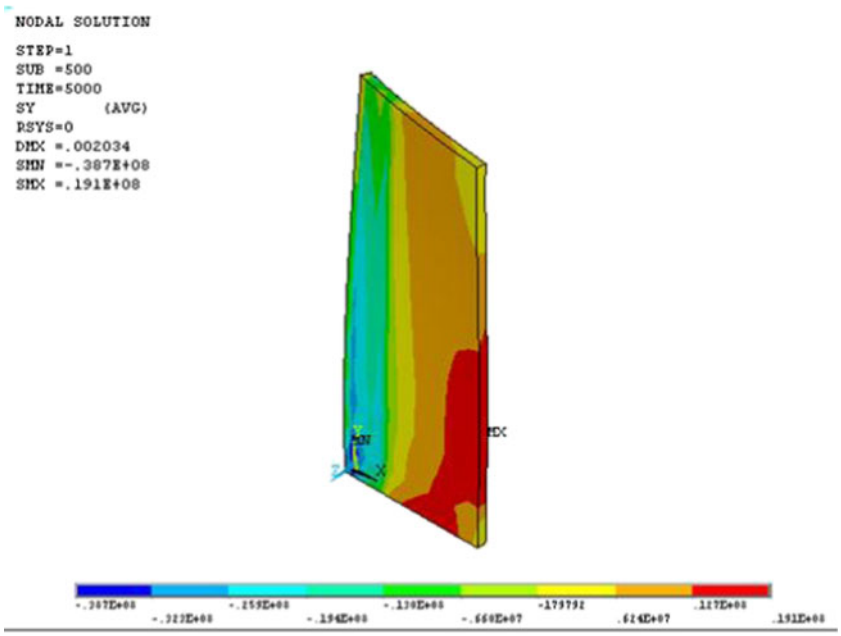

Fig. 19 Residual stress plot along *y*-axis (case 2)

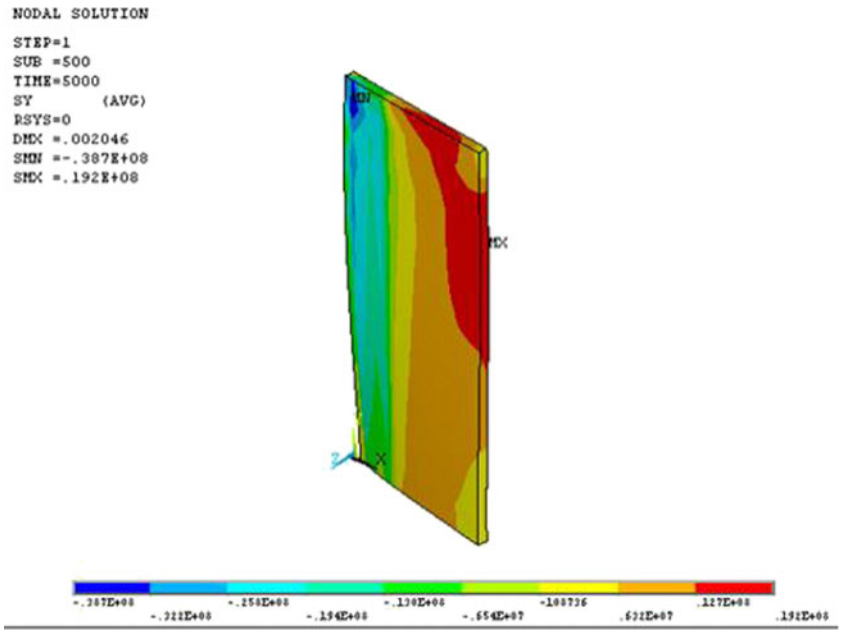

Fig. 20 Residual stress plot along *y*-axis (case 3)

Thermal analysis results show that the temperature distribution in the longitudinal direction (along the welding line) does not vary considerably since the constant temperature is applied at the weld joint during analysis, but the temperature varies significantly in the transverse direction. These changes of transient temperature will significantly affect the forming and developing of the residual stresses.

The mechanical response of the plate for the three different cases show a significant influence on transversal stresses; especially regarding a path transverse to welding line at the middle of the plate. The results for constraints (for both cases 2 and 3) fixed at transverse direction to welding line present a relatively small stress about 70 MPa, which is much less than the yield strength of the plate, i.e., the elastic behavior is the governing mechanism for the stress field. The plate fixed at the side edge parallel to the welding line (case 1) has a stress level about 460 MPa which is greater than the yield strength, i.e., the plastic behavior is the governing mechanism for the stress field. Altogether, results are expected that along the welding line, transverse stresses are almost the same for three different constraints and peak value of the stress is less than the yield strength. From these results, it can be concluded that there is no influence on residual stresses for two boundary constraints (cases 2 and 3), but a significant effect on residual stresses in case 1. Therefore, cases 2 and 3 are more suitable for applying boundary constraints to reduce the residual deformation. Residual deformation is very small in the three different cases.

The residual stress is found to be directly proportional to the plate thickness, when heat source input and material properties are same in case 1. The residual stresses are very little different due to different mesh models, when heat source input, material properties are the same in case 1. The residual stress is found to be directly proportional to the material properties, when heat source input and mesh are the same in case 1.

Acknowledgments This work has been made under the plurianual funding of the Portuguese Foundation of Science and Technology (Fundação para Ciência e Tecnologia) to the Centre for Marine Technology and Engineering (CENTEC).

References

1. Adak M, Mandal NR (2009) Pseudolinear equivalent constant rigidity concept for analyzing welding deformations. Appl Math Model 33:2096–2108
2. Adak M, Mandal NR (2010) Numerical and experimental study of mitigation of welding distortion. Appl Math Model 34: 146–158
3. Al-Mulhim K, Said SAM, Yibas BS, Habib MA, Al-Bagawi J (2002) Multi-dimensional transient heat conduction in heat exchanger tube sheets. Proc Inst Mech Eng Part B: J Eng Manuf 216:331–345
4. ANSYS, Inc. (2002) Theory reference, ANSYS Inc.
5. Argyris JH, Szimmat J, William KJ (1982) Computational aspects of welding stress analysis. Comput Methods Appl Mech Eng 33:635–666
6. Biswas P, Mandal NR, Sha OP (2007) Three dimensional finite element prediction of transient thermal history and residual deformation due to line heating. J Eng Marit Environ 221:17–30
7. Dong Y, Hong JK, Tsai CL, Dong P (1997) Finite element modeling of residual stresses in austenitic stainless steel pipe girth welds. Weld J 76:442s–449s
8. Fanous FZI, Younan YA, Wifi SA (2003) Study of the effect of boundary conditions on residual stresses in welding using element birth and element movement techniques. J Press Vessel Technol 125: 432–439
9. Hibbitt HD, Marcal PV (1973) A numerical thermo-mechanical model of the welding and subsequent loading of a fabricated structure. Comput Struct 3:1145–1174

10. Ji SD, Fang HY, Liu SX, Meng QG (2005) Influence of a welding sequence on the welding residual stress of a thick plate. Model Simul in Mater Sci Eng 13:553–565
11. Karlsson L (1986) Thermal stresses in welding. In: Hetnarski RB (ed) Thermal stresses. Elsevier, Amsterdam, pp 299–389
12. Kristina A et al (1990) Artificial neural network applied to arc welding process modeling and control. IEEE Trans Ind Appl 26: 824–830
13. Long H, Gery D, Carlier A, Maropoulos PG (2009) Prediction of welding distortion in butt joint of thin plates. Mater Des 30:4126–4135
14. Marstruct (2009) Benchmark studies on distortions and residual stresses, 1-58. Report MARSTRUCT project
15. Masubuchi K (1980) Analysis of welded structures. Pergamon Press, Oxford, UK
16. Murakawa H, Ueda Y, Zhong XM (1995) Buckling behavior of plates under idealized inherent strain. Trans JWRI 24:87–91
17. Papazoglou VJ, Masubuchi K (1982) Numerical analysis of thermal stresses during welding including phase transformation effects. J Press Vessel Technol 104:198–203
18. Rosenthal D (1946) The theory of moving sources of heat and its application to metal treatment. Transactions of ASME 68:849–866
19. Rybicki EF, Schmueser DW, Stonesifer RB, Groom JJ, Mishler HW (1978) A finite element model for residual stresses and detections in girth-butt welded pipes. J Press Vessel Technol 100:256–262
20. Sunar M, Yilbas BS, Boran K (2006) Thermal and stress analysis of a sheet metal in welding. J Mater Proc Tech 172:123–129
21. Tekriwal P, Mazumder J (1988) Finite element analysis of three dimension transient heat transfer in GMA welding. Weld J 67: 150s–156s
22. Tekriwal P, Mazumder J (1991) Transient and residual thermal strain-stress analysis of GMAW. J Eng Mater Technol 113:336–343
23. Teng TL, Chang PH, Tseng WC (2003) Effect of welding sequences on residual stresses. Comput Struct 81:273–286
24. Watanabe M, Satoh K (1961) Effect of welding conditions on the shrinkage distortion in welded structures. Weld J 40:377s–384s
25. Zhu XK, Chao YJ (2002) Effects of temperature dependent material properties on welding simulation. Computers and Structures 80:967–976